Development of a Self-Calibrating X-ray Detector for Accelerator Diagnostics

Luciano Malavasi
Department of Physics, Worcester Polytechnic Institute
Department of Physics,
University of California Santa Barbara (Physics REU 2022)
lkmalavasi@wpi.edu

Patrick Moriishi Freeman, Brunel Odegard, and David Stuart
Department of Physics, University of California Santa Barbara
(Dated: October 14, 2022)

A modular, low-cost, small footprint silicon photomultiplier (SiPM) based x-ray detector is being developed to continuously measure drift gap endpoint energy at the Los Alamos Neutron Science Center (LANSCE) Drift Tube LINAC (DTL). The proposed design will be manufactured in large quantities to be installed along the length of the DTL to measure the spectrum of x-ray bremsstrahlung from field-emitted electrons inside the accelerator RF cavity. The detector is capable of in-situ self-calibration from the radioactive self-activity of LYSO scintillator crystals. This report summarizes preliminary results characterizing the performance of a detector prototype installed and tested at LANSCE July 30th-August 3rd, 2022.

I. INTRODUCTION

Developing robust instrumentation for experiments in high energy physics ensures the reliability of particle accelerators and the accuracy of data collection in nuclear and high energy physics experiments. Broadly, initiatives in instrumentation can be categorized as either detection systems, that operate near the primary beam target and collision site, or diagnostic systems that monitor the conditions of various components of the accelerator along the beamline and assist in calibration or error correction.

A typical diagnostic challenge for drift tube linear accelerators (DTL) consists of measuring the endpoint energy of a drift gap. In this report, we propose the design of an x-ray detector module that continuously monitors the DTL gap energy by collecting the x-ray bremsstrahlung spectrum in the accelerator cavity. We construct a prototype of the proposed detector and characterize its performance with known x-ray sources as calibration data.

Recent advances in solid-state optoelectronics have seen the development of silicon photomultiplier (SiPM) sensors, which consist of a parallel array of single-photon avalanche diodes, as an alternative photodetection system to traditional photomultiplier tubes (PMT). Compared to PMTs, SiPMs feature similarly high gain, photodetector efficiency, time resolution, and sensitivity to single-photon events, with a much smaller physical footprint, lower cost, and lower operating bias voltage [1].

A. Drift tube linear accelerators

DTL structures accelerate charged particles with radio frequency (RF) electrical power through a series of drift tubes separated by gaps of varying widths (Fig. 1). The drift tubes are connected to the RF power in alternating phases. When the charged particle is moving through the gap between drift tubes, the electric field across the drift tube gap accelerates the particle. When the direction of this electric field reverses, the particle enters an equipotential region inside a drift tube and experiences zero deceleration.

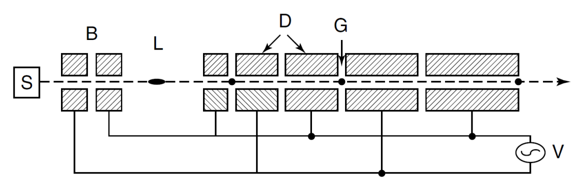

FIG. 1: Diagram of a DTL from Ref. [2]. S is the beam source, D are the drift tubes, G are the gaps

In the resonant cavity of a DTL, the RF electric fields generate field-emitted electrons (FEE). The FEEs are accelerated by the potential difference V_{gap} across the drift tube gap and collide with the subsequent drift tube, producing x-ray bremsstrahlung from the Coulombic interactions. This process is illustrated in Fig. 2 [3]. The resulting x-ray spectrum is a distribution of photon energies up to the maximum kinetic energy of electrons accelerated across this gap, $T = eV_{gap}$. X-ray spectroscopy therefore represents an avenue for designing instrumentation to monitor DTL gap energies.

DTLs are commonly used as injectors in many accelerator facilities. For example, LINAC4 at CERN is a DTL that supplies 160 MeV H$^-$ ions to the Large Hadron Collider proton storage systems. In other cases, DTLs comprise a primary acceleration stage for a LINAC. At LANSCE, the DTL stage provides the first 100 MeV of acceleration for the 800 MeV beamline. The LANSCE DTL is composed of four resonant RF tanks at an operating frequency of 201.25 MHz.

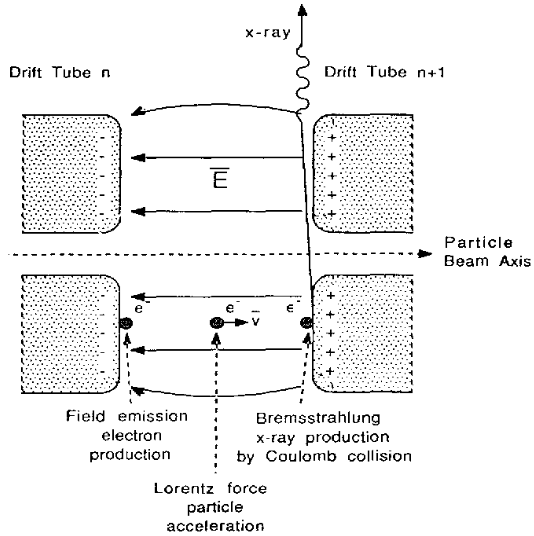

FIG. 2: Schematic of field-emitted electrons inside a DTL. From Ref. [3]

II. DESIGN

A. LYSO+SiPM-based prototype

A general block diagram of the LYSO+SiPM-based detector is outlined in Fig. 3. An incoming x-ray strikes a scintillator, which produces a cascade of low-energy (near-UV) photons. This light signal is accepted by a silicon photomultiplier (SiPM) detector, producing photocurrent that undergoes gain and filtering before undergoing analog-to-digital conversion and serialization. Readout, control, and in-situ analysis is performed with a Raspberry Pi v4. The system is designed with three physical modules: a sensor, analog signal processing, and a digitizer.

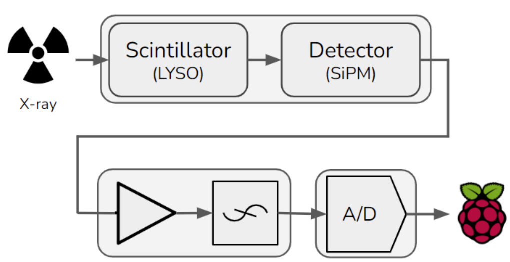

FIG. 3: A block diagram of the x-ray detector

a. Sensor The sensor module consists of a pair of 4x4x22 mm LYSO scintillator crystals mounted on 4x4 mm AdvanSiD ASD-NUV4S-P SiPMs. The printed circuit board (PCB) for the sensor module (Fig. 5) has a physical footprint of 35x42 mm. Relative to PMTs, the small sensor footprint minimizes the volume of material required to shield the sensor and collimate incoming x-rays.

Single-photon avalanche diodes, which form a SiPM sensor, are photosensitive p-n junctions reverse-biased beyond the breakdown voltage. From Ref. [1], an approximate threshold voltage for reverse breakdown is 28 V (Fig. 4), significantly lower than bias voltages necessary for PMT operation.

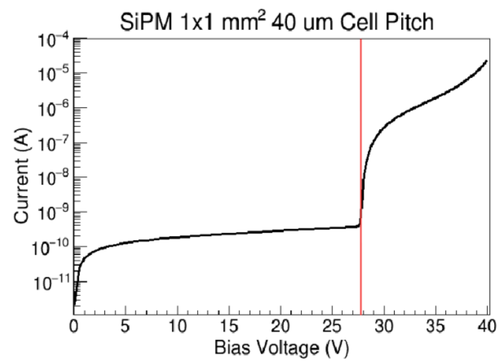

FIG. 4: I-V curve for a 1x1 mm^2 SiPM from Ref. [1]. Breakdown occurs at about 28 V reverse bias

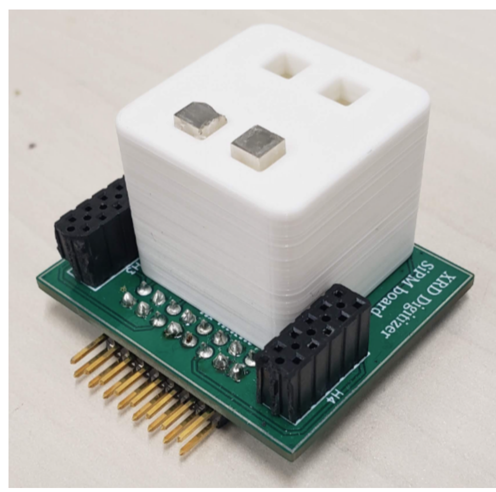

FIG. 5: The sensor module. Two 4x4x22 mm LYSO crystals are mounted on 4x4 SiPMs

b. Analog processing The analog processing module consists of a photocurrent sense resistor, an operational amplifier (opamp) voltage buffer, and a non-inverting opamp gain stage. A single module contains two signal chains for processing the pair of SiPMs on the sensor module. A minimized schematic of a single channel of the module is given in Fig. 6, and an assembled prototype of the analog processing module is shown in Fig. 7 A complete schematic and PCB layout diagram can be found in in Appendices A and B.

c. Digitizer In prototype testing, waveform sampling and digitization was performed with a Paul Scherrer Institut DRS-4 evaluation board [4], a 700 MHz, 0.7 GS/s USB oscilloscope with a memory depth of 1024 samples.

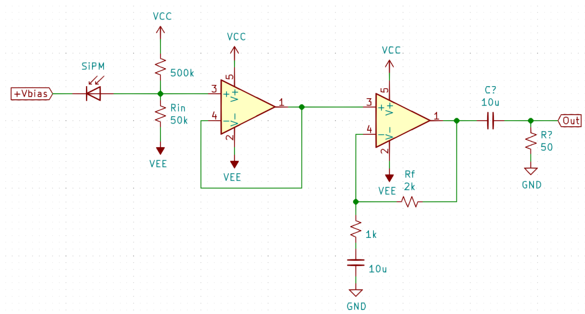

FIG. 6: Schematic of one channel of the analog processing module

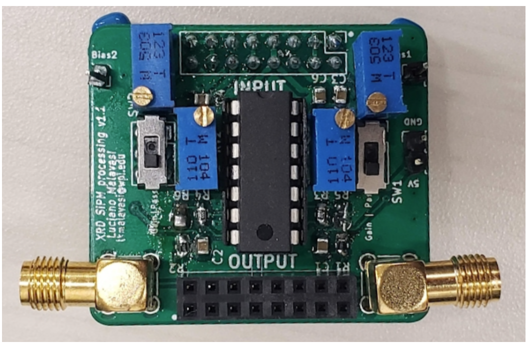

FIG. 7: Analog processing board prototype

In the final application, the digitizer module is a custom [5] analog-to-digital waveform readout board with 32 MHz sampling, built-in trigger logic, and I2C control of SiPM biasing. It samples the wavefunction with an 8-bit ADC and stores 4 KiB (4096 events, 128 μs) of waveform data per channel per event in SRAM for readout. The board also makes use of I2C-addressable digital potentiometers to adjust the output voltage of a boost converter to bias SiPMs. Software-configurable event triggering is handled with analog comparators between the input signal and a reference voltage from an I2C-addressable DAC. Configurable trigger logic is controlled with a PWM pin to set the Boolean trigger condition between both channels.

B. LaBr-based prototype

Another detector is being developed in parallel, using a lanthanum bromide (LaBr) scintillator coupled to a PMT. The detector also contains a LYSO crystal coupled to a separate PMT for self-calibration. LaBr potentially offers improved energy resolution compared to LYSO, though the PMT used for light collection results in a larger form factor which requires more extensive shielding and the components are not as cost effective.

III. EXPERIMENTAL SETUP

The performance of the prototype detector module was characterized ex-situ by collecting the radioactive emission spectra of ^{133}Ba, ^{57}Co, and ^{22}Na sources. These calibration sources were selected due to their clearly-defined emission peaks in energy ranges roughly corresponding to the expected gap energy of a DTL (on the order of 50-500 keV). The experimental setup is shown in Fig. 8. Spectra were collected at a range of SiPM bias voltages and amplifer gain values for characterization; in-situ tests were conducted at 30.5 V bias to maximize internal SiPM gain.

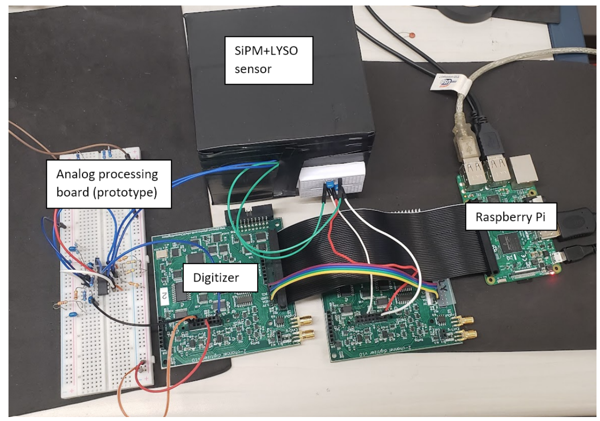

FIG. 8: Prototype detector test setup

Significant undesired x-ray signal from adjacent RF tanks at the DTL was anticipated from prior experiments. [6]. To account for this, the module was wrapped laterally with lead ribbon to shield the sensor (Fig. 9). We additionally wrapped the sensor enclosure in grounded adhesive copper ribbon for EM shielding.

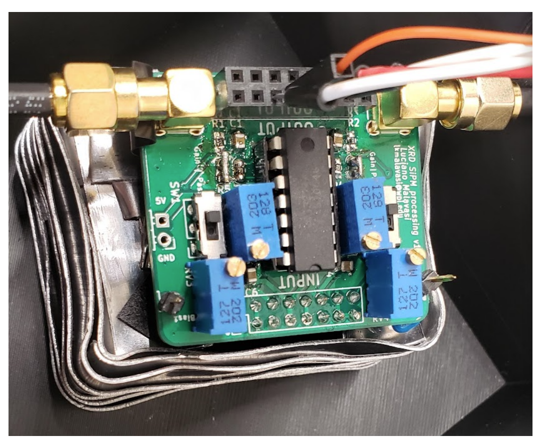
FIG. 9: The sensor module (wrapped in lead tape) coupled to the analog processing module

During in-situ testing, two modules were installed for comparison. One module was surrounded with lead bricks to maximize shielding robustness, while the other was only shielded by the lead tape. SiPM bias voltage and analog gain was kept consistent across all channels.

The LANSCE DTL beamline passes through four consecutive resonant RF tanks, operating at 201.25 MHz. The detector assembly was installed near the beginning of tank 2 (Fig. 10. We collected x-ray spectra with RF turned off, with each tank individually on, with all tanks turned on, and with just the background tanks (tanks 1, 3, and 4) turned on. Additionally, we measured the spectra of tank 2 at intermediate stages as the RF power was increased to its normal operating level.

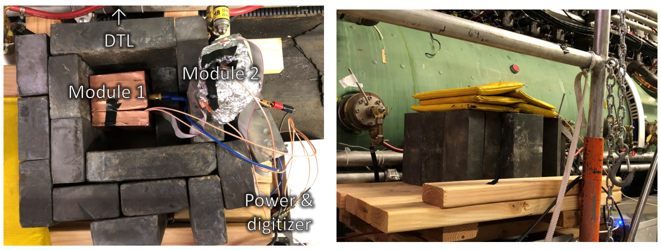

(a) Top view

(b) Side view

FIG. 10: Prototype x-ray detector module installed near tank 2 at the LANSCE DTL

IV. RESULTS

A. Ex-situ characterization

A histogram of waveform areas collected with ^{133}Ba, ^{57}Co, and ^{22}Na sources is shown in Fig. 11. We can clearly resolve a distinct peak in the ^{22}Na spectrum at approximately 400 nV·s, corresponding to the 511 keV radioactive peak. Likewise, we are able to resolve the 356 keV (∼270 nV·s) peak in the ^{133}Ba spectrum, and the 122 keV (∼90 nV·s) ^{57}Co peak.

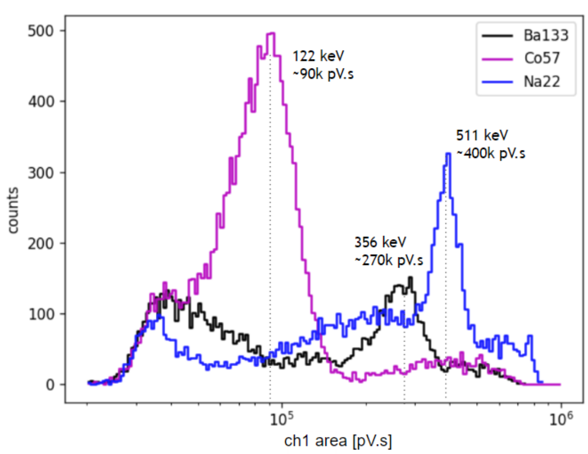

FIG. 11: Ex-situ spectroscopy of three x-ray sources

We investigated the efficacy of lead tape shielding by collecting ^{133}Ba spectra with the source placed adjacent to the sensor body with increasing lead thicknesses. The event rate was monitored at each layer of lead, until the mean event rate achieved a stable minimum value of around 150 Hz. This corresponds primarily to the self-activity of LYSO, with a slight contribution from the x-ray background of the testing environment. A comparison of the event rate histogram with and without lead tape shielding as recorded by the DRS-4 hardware scalers is shown in Fig. 12. The reported hardware scaler histogram with no source contributing to the x-ray activity is overlaid on Fig. 12b for comparison, scaled to contain the same number of events as the plot with a source.

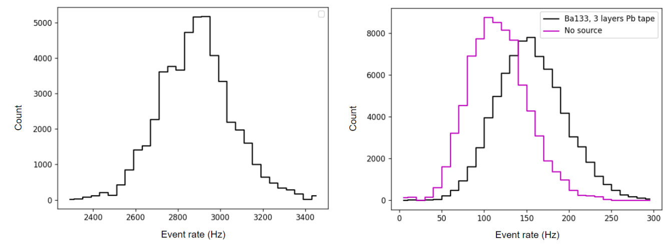

(a) No lead shielding, ∼2800 Hz events

(b) 1.8 mm lead shielding, ∼150 Hz events

FIG. 12: A comparison of event rates before (a) and after (b) adding 1.8 mm of lead tape shielding

B. In-situ testing

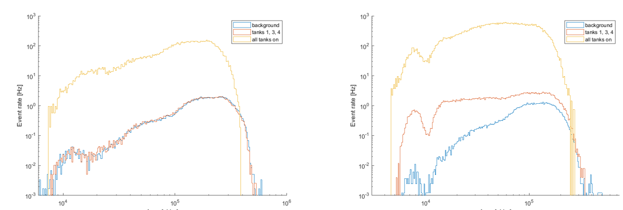

(a) Module 1 spectra (Pb brick shielding)

(b) Module 2 spectra (Pb tape shielding)

FIG. 13: X-ray spectra in modules 1 and 2 with RF off (blue), peripheral tanks at full power (red), and all tanks at full power (yellow)

With the two modules installed at the DTL, we collected a calibration background spectrum with the RF off. Then, spectra were collected in both modules with each tank individually turned on to their respective operating power. Data was also collected for tank 2 at intermediate power points: 1.20 MW (50.4% of the 2.38 MW full power), 1.61 MW (67.6% power), and 1.89 MW (79.4% power). A spectrum with all the peripheral tanks (tanks 1, 3, and 4) at full power and all four tanks at full power was collected.

To produce the spectra obtained in Fig. 13, the collected x-ray pulse area histograms were scaled vertically to represent incident x-ray event rate. The scale factor applied is the ratio between the mean hardware scaler recorded by the DRS-4 and the total event count in the histogram, after applying cuts that exclude coincident events (LYSO self-activity) and noise events. As expected, module 1 completely rejected any signal from peripheral tanks (Fig. 13a). By contrast, module 2 received somewhat steady signal from tanks 1, 3, and 4, represented by the delta between the the background and peripheral tanks spectra in Fig. 13b. In both modules, the signal received from tank 2 (delta between peripheral signal and signal from all tanks) was two orders of magnitude stronger than the background signal, rendering any background signal negligible to within 1%.

We investigate how each peripheral tank contributes to the unwanted background signal. The module 2 spectrum of each individual peripheral tank plotted in comparison with the spectrum of the three tanks combined and the background RF is presented in Fig. 14. The background signal was subtracted from each spectrum to isolate the x-ray spectrum of each tank (Fig. 15).

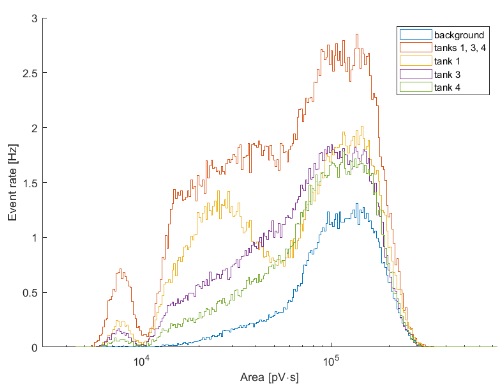

FIG. 14: Individual contributions of each peripheral tank to the unwanted spectrum measured in module 2

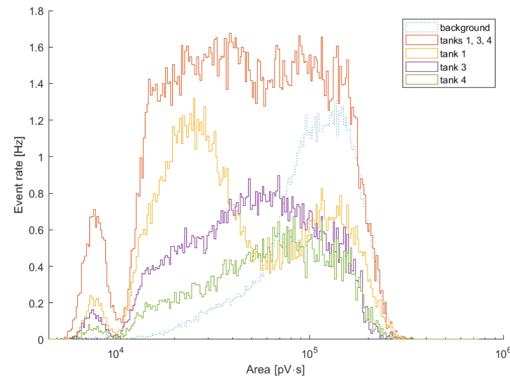

FIG. 15: The individual contributions of each tank are isolated by subtracting the background spectrum from measured spectra in Fig. 14

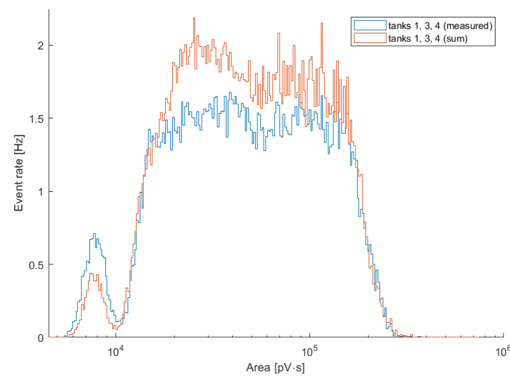

FIG. 16: Reconstructing the measured peripheral signal in module 2 by summing spectra of individual peripheral tanks (with background subtraction)

It is not apparent that any particular tank is contributing more significantly to the background spectrum than any others, apart from a slightly higher rate of lower energy events in tank 1. This result supports continuing to pursue robust isotropic shielding solutions. In particular, one extension to the current shielding structure is to manufacture a collimation shield that narrows the sensor field of view, potentially improving the accuracy of the sensor to individual drift gaps.

To verify the consistency of our data, we sum the isolated spectra of Fig. 14 and compare the reconstructed peripheral signal to the measured spectrum with tanks 1, 3, and 4 on. There is close agreement between the reconstructed background signal and the measured background signal in Fig. 16, indicating no significant change in gain or loss of signal across several data collection runs.

The difference in magnitude between the reconstructed signal and the measured background signal remains to be investigated, but may be an artifact from the scaling factors applied to each spectrum to convert raw histograms to event rates.

V. DISCUSSION

X-ray detection represents an effective method of performing accelerator diagnostics. We developed and characterized a silicon photomultiplier-based x-ray detection prototype capable of continuous data acquisition, at a significantly smaller price and footprint compared to photomultiplier tube and high purity germanium detectors.

The prototype detector was characterized ex-situ by performing spectroscopy on common radioactive x-ray sources. Additionally, we investigated the efficacy of shielding with lead ribbon by simulating peripheral signal with x-ray sources and increasing the shielding thickness until only background signal was received. Two detector modules were installed for in-situ testing at LANSCE.

The results from the testing demonstrate that measuring the spectrum of tank 2 while effectively rejecting x-rays from peripheral tanks is possible with lightweight, small, and inexpensive shielding solutions. The measured signal from tank 2 was two orders of magnitude stronger than the measured signal from background and peripheral tanks combined. Though this prototype shielding solution is successful, improved detector accuracy and reliability is obtainable by manufacturing a more robust shielding apparatus that collimates the sensor field of vision. We also investigated the consistency of the detector by reconstructing the measured spectrum of peripheral tanks from the sum of spectra of individual tanks.

As we move to a finalized detector design, we will continue testing and improving various aspects of the detector signal chain. We will investigate methods for optimizing the LYSO+SiPM sensor energy resolution by integrating reflective coating and improving optical coupling of the scintillator to the SiPM. We also plan to implement additional data acquisition features such as event rate monitoring to the custom digitizer board. A finalized module will be used to demonstrate the feasibility of in-situ self-calibration from the self-activity of LYSO to SiPM modules, which has previously only been implemented on PMT-based systems.

A finalized and calibrated design would involve the parallel operation of possibly hundreds of such detectors installed semi-permanently along a DTL beamline. Compared to current x-ray detection diagnostic systems, this design is smaller and lower cost, operates without the use of high bias voltages or cryogenic cooling, and can be installed semi-permanently for continuous data acquisition during accelerator operation. If such a detector proves to be an effective and reliable diagnostic tool, the design would be applicable in other DTL systems.

ACKNOWLEDGMENTS

I would like to acknowledge the gracious support and guidance of Dr. Sathya Guruswamy and my advisor Dr. David Stuart, who enabled me to participate in this REU by organizing the program and hosting me in the Stuart Group laboratory. Their expertise and advice was invaluable in the research process. I would also like to thank my post-doctoral mentor Dr. Patrick Moriishi Freeman and graduate mentor Brunel Odegard, for teaching me the physics underpinning this project and tirelessly answering questions. This research experience was generously sponsored by the National Science Foundation (NSF) REU grant PHY-1852574.

Appendix A: Analog processing module schematic

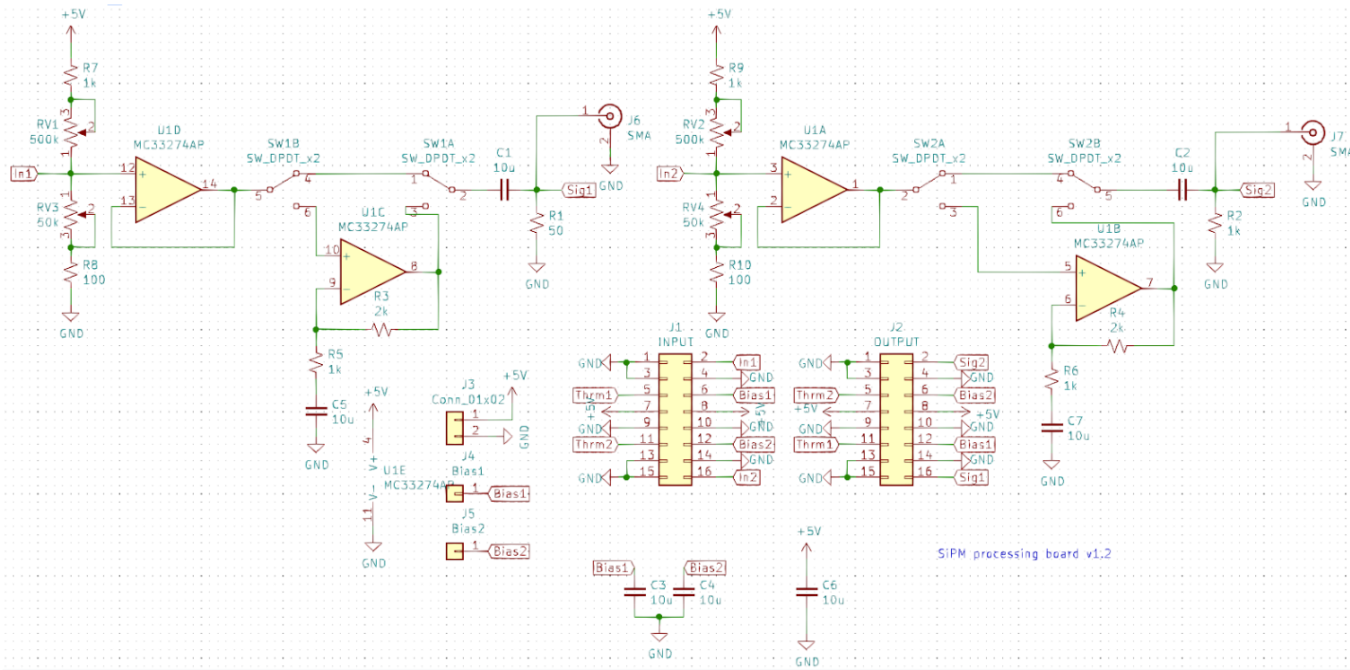

Appendix B: Analog processing module PCB

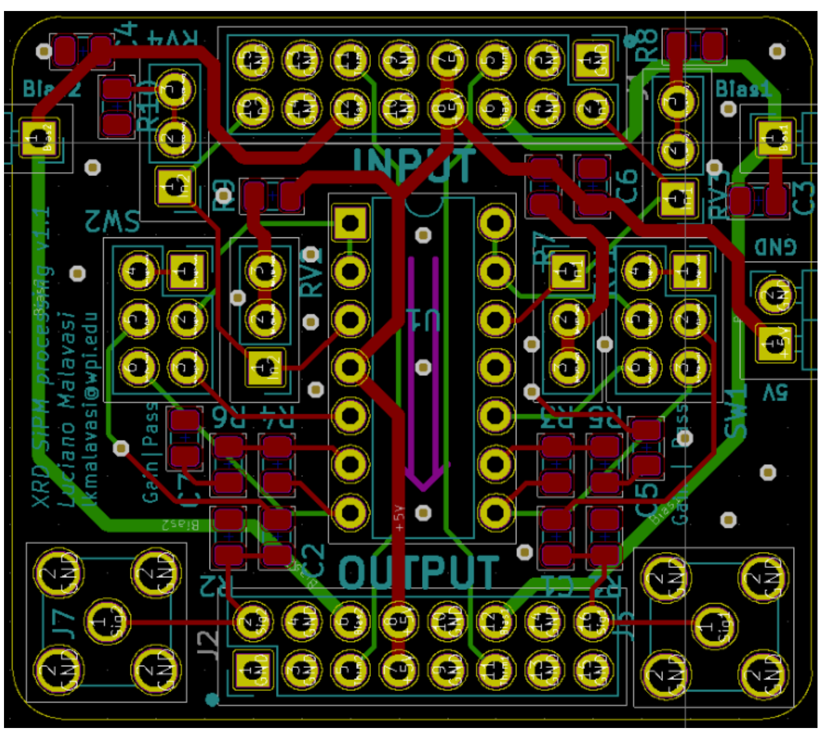

Appendix C: Definitions

DTL: Drift tube LINAC
FEE: field-emitted electron
LANSCE: Los Alamos Neutron Science Center
LINAC: linear accelerator
LYSO: Lutetium–yttrium oxyorthosilicate scintillation crystal
PMT: photomultiplier tube
RF: radio frequency
SiPM: silicon photomultiplier

[1] G. Zappalà, F. Acerbi, A. Ferri, A. Gola, G. Paternoster, N. Zorzi, and C. Piemonte, Set-up and methods for SiPM Photo-Detection Efficiency measurements, Journal of Instrumentation **11** (08), publisher: IOP Publishing.
[2] T. P. Wangler, Rf linear accelerators (Wiley-VCH Verlag, 2017) p. 3.
[3] G. O. Bolme, G. P. Boicourt, K. F. Johnson, R. Lohsen, O. R. Sander, and L. S. Walling, Measurement of RF Accelerator Cavity Field Levels at High Power From X-ray Emissions· (1990).
[4] https://www.psi.ch/en/drs/evaluation-board.
[5] http://dstuart.physics.ucsb.edu/2ChannelDigitizer/.
[6] M. Sanchez Barrueta, G. Bolme, J. Lyles, R. Pinsky, and J. Zane, X-Ray Detector Array for Spatial and Temporal Diagnostic at the LANSCE Linac, Proceedings of the North American Particle Accelerator Conference **NAPAC2019**, 10.18429/JACOW-NAPAC2019-MOYBB6 (2019), publisher: JACoW Publishing, Geneva, Switzerland.